JOURNAL OF MATERIALS SCIENCE 27 (1992) 3108–3117

Nucleation and growth of ion beam sputtered metal films

SHI XU, B. L. EVANS
J. J. Thomson Physical Laboratory, University of Reading, Whiteknights, Box 220, Reading, Berks RG6 2AF, UK

Transmission electron microscope observations have been made on ion beam sputtered (IBS) films of Cu, Au, Pt and Ni (of predetermined thickness $t' \geqslant 0.5$ nm) deposited on amorphous carbon substrates. The influence of IBS parameters on particle size distribution and deposition rate has been measured, also the fractional substrate coverage f as a function of t' which indicates three-dimensional island growth in Au, Cu films and two-dimensional growth in Pt, Ni films. Electron diffraction measurements appear to show that the f.c.c. metal particles grow with (1 1 0) parallel to the substrate with, in the case of Ni, a critical island thickness of ~ 0.8 nm.

1. Introduction

The nucleation and growth of metal films has been a subject of study for many years, as described in recent review articles [1, 2]. Metal films may be deposited on substrates by a number of different techniques such as thermal evaporation, sputtering, plasma decomposition etc., but whichever method is employed it is necessary to have close control over the deposition parameters so that their individual influence on the growth processes can be observed. It is for this reason that thermal evaporation of the metal from a Knudsen cell in ultra-high vacuum is often the preferred method, the metal vapour condensing on a freshly cleaved single-crystal substrate surface maintained at a known temperature. Under these conditions the deposition parameter is the vapour beam flux which is controlled by the source temperature.

Another technique which is capable of producing a well-defined flux of metal atoms is that of ion beam sputtering (IBS) in which inert gas atoms are directed on to a metal target surface. The metal atoms ejected from the target are then deposited on a substrate which is out of the "line of sight" of the ion gun. In this method the number and energies of the metal atoms arriving at the substrate may be varied but the film deposition rates are very low, typically 0.4 nm min^{-1}. This has the advantage that the deposition can be terminated at a very early stage in the substrate coverage, which allows initial stages of film growth to be observed.

In general the growth of a solid film on a substrate takes place in one of three ways which depend, primarily, on the relative values of the adatom–adatom (cohesive) and adatom–substrate atom (adhesive) interaction energies. These are (i) the island, or Volmer–Weber [3] growth mode in which small clusters nucleate on the substrate surface and grow into islands of the condensed phase; this occurs when the cohesive energy exceeds the adhesive energy; (ii) the layer, or Frank–van der Merwe [4–6] growth mode in which the adhesive energy is greater than the cohesive so that the first atoms form a complete monolayer (ML) on the substrate surface which is followed by a second ML and so on, provided the decrease in binding energy is monotonic towards the bulk crystal value; (iii) an intermediate layer plus island, or Stranski–Krastanov [7] growth mode in which after the first few MLs the energetics favour island growth.

Lattice matching between the deposited film and the crystalline substrate favours epitaxial layer growth but where this does not occur, as in the case of metals on alkali halides, MoS_2, MgO, mica and graphite [2], island growth predominates although this can be modified by the degree of supersaturation as influenced by the deposition rate and substrate temperature [8–11]. When island growth does occur the nucleation density is profoundly affected by defects on the substrate surface. This is because the adatom binding energy at a defect is greater than on the open surface, as evidenced by the metal decoration which reveals growth steps and dislocations at the surface of alkali halide crystals (e.g. [12]).

The experiments to be described in this paper were made on IBS metal films deposited on thermally evaporated carbon substrates. All the available evidence indicates that these carbon film substrates are amorphous. As such the substrate surface is unlikely to be atomically smooth. However, the reproducible behaviour of each metal film indicates that any sample-to-sample variation in surface defect concentration is not significant. It is the markedly different growth behaviour of the series of face-centred cubic (f.c.c.) metals Ni, Pt, Au, Cu on amorphous carbon (a-C) substrates that is of interest here.

2. Experimental procedure

The a-C substrates, thickness 20 nm, were prepared by

0022–2461

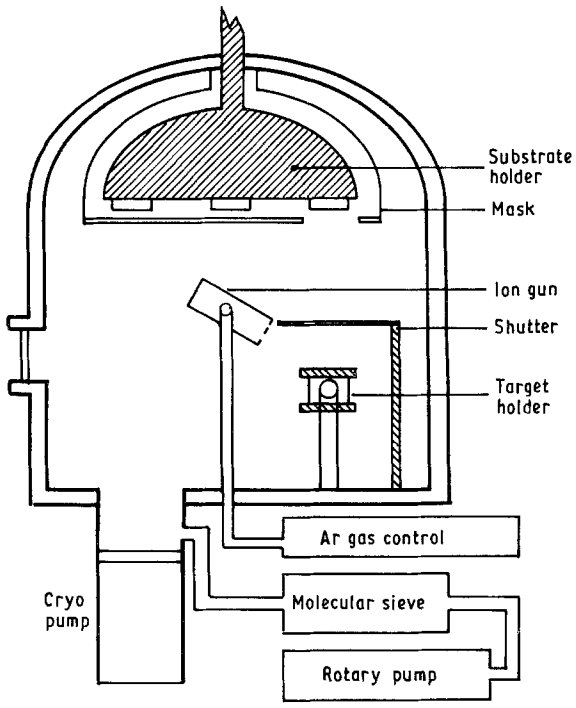

Figure 1 IBS deposition system.

carbon arc evaporation on to the surface of freshly-prepared sodium chloride crystals grown from Analar solution. When immersed in water the carbon film floated free from the crystal and could be transferred to an electron microscope (EM) grid.

The carbon-coated EM grids were positioned in the deposition chamber, shown schematically in Fig. 1, which was then cryopumped to a pressure of less than 5×10^{-5} Pa. When high-purity Ar gas was admitted to the ion gun, the dynamic Ar gas pressure within the continuously pumped chamber increased to 6.6 $\times 10^{-2}$ Pa. A d.c. voltage was applied to the ion gun to initiate the discharge and the Ar gas supply adjusted (and subsequently computer-regulated) to give the required value of ion gun voltage V_g. The ion gun current I_g was determined by the stabilized ion gun power supply.

The flux of inert gas ions and excited atoms from the ion gun was incident on the target at an angle of 60° to the normal. After sputter-cleaning the metal target for some hours, the shutter was opened so that the sputtered target atoms were deposited on the carbon-coated EM grids positioned vertically above the target (Fig. 1). Closing the shutter determined the end of the deposition time, T.

2.1. Measurement of film deposition rate

For the measurement of deposition rate the films were deposited on the chemically cleaned (1 1 1) surface of electropolished (electronic grade) silicon wafers. For each chosen sputtering condition at least three samples of different thicknesses t were prepared, two for Talystep measurement ($t > 20$ nm) and one for soft X-ray interference measurements ($t < 20$ nm).

In the Talystep measurements t was determined by traversing the stylus across the sharp film "edge" produced by a mask which had been held in intimate contact with the silicon substrate. For the soft X-ray measurement of film thickness, the sample was mounted in a vacuum spectrometer and the intensity of the radiation (wavelength $\lambda = 0.834$ nm) reflected from the metal film recorded as a function of glancing angle of incidence ϕ. Maxima in the reflected intensity due to constructive interference between waves reflected at the top (metal–vacuum) and bottom (metal–silicon) interfaces occur when

$$2t \sin\phi \left(1 - \frac{\delta}{\sin^2\phi}\right) = \left(p + \frac{1}{2}\right)\lambda \qquad (1)$$

where $p = 0, 1, 2$, etc. The refractive index decrement δ in Equation 1 is given by $n_1 = (1 - \delta)$ where n_1, the real part of the complex metal refractive index at $\lambda = 0.834$ nm, can be obtained from the listed values of the atomic scattering factors [13]. Plotting the fringe order number p versus $\sin\phi\ [1 - (\delta/\sin^2\phi)]$ gives a straight line from which t is determined. At the wavelength employed ($\lambda = 0.834$ nm) this method can be used for $t > 6$ nm. For smaller values of t it is necessary to utilize metal/a-C multilayers (see section 3.2.2).

In the case of IBS carbon films the soft X-ray amplitude reflectivity at the carbon–silicon interface is too small to give observable interference effects. This was overcome by constructing metal–carbon–metal etalons, the thickness of the thin metal layers being known from the previously measured metal deposition rate. For such an etalon reflectivity maxima occur when

$$2d \sin\phi \left(1 - \frac{\bar{\delta}}{\sin^2\phi}\right) = p\lambda, \qquad p \text{ integer} \qquad (2)$$

where $d = t_m + t_c$ is the thickness of a layer of metal (t_m) and a layer of carbon (t_c). The mean refractive index decrement $\bar{\delta} = \gamma\delta_m + (1 - \gamma)\delta_c$ where $\gamma = t_m/d$. Plotting the measured values of ϕ as p versus $\sin\phi\ [1 - (\bar{\delta}/\sin^2\phi)]$ gives the value of d and hence t_c. For maximum accuracy the value of t_m should be as small as is consistent with a continuous metal film.

When three or more different film thicknesses had been prepared and measured a graph of thickness versus deposition time was plotted, an example of which is given in Fig. 2; the slope of this graph gives the deposition rate appropriate to a particular set of sputtering parameters. The deposition rates R of Pt, Ni, Cu, Au and carbon films were measured for different ion gun voltage, V_g, at constant ion gun current I_g and for different I_g at constant V_g.

2.2. Transmission electron microscope (TEM) observations

The metal films deposited on the carbon-coated EM grids were examined using a Hitachi H-800 TEM operating at 200 kV. Bright-field images (magnification 3×10^5) and electron diffraction patterns were recorded; the diffraction aperture was such that an area 5 cm diameter (of the 3×10^5 TEM picture) contributed to the diffraction pattern. During examination in the TEM there was no evidence of any

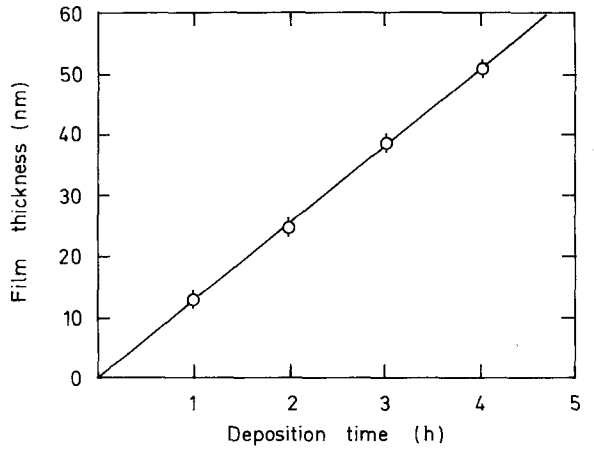

Figure 2 IBS Pt films deposited on (1 1 1) Si. Measured values of the Pt film thickness versus deposition time ($V_g = 2.2$ kV, $I_g = 260$ mA).

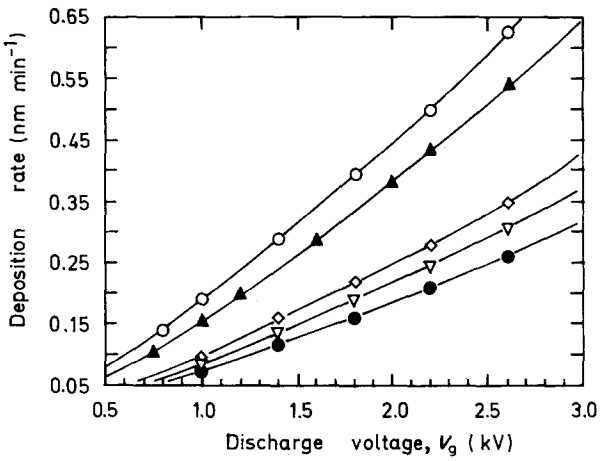

Figure 4 Measured deposition rate of (○) Cu (220 mA), (▲) Au (220 mA), (◇) Ni (260 mA), (▽) Ni (220 mA) and (●) Pt (260 mA) films versus ion-gun (discharge) voltage V_g for the indicated ion-gun currents I_g.

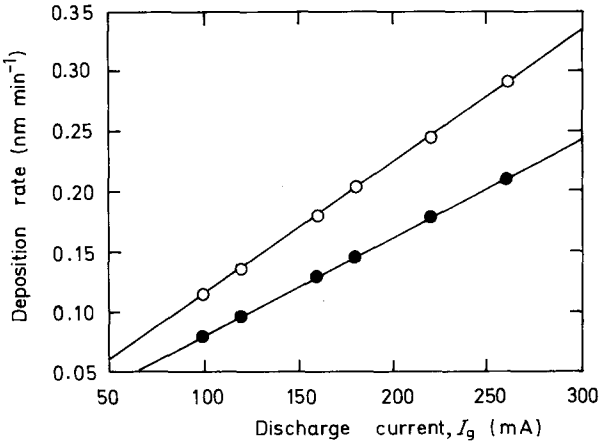

Figure 3 Measured deposition rate of (○) Ni and (●) Pt films versus ion-gun (discharge) current I_g at ion-gun voltage $V_g = 2.2$ kV.

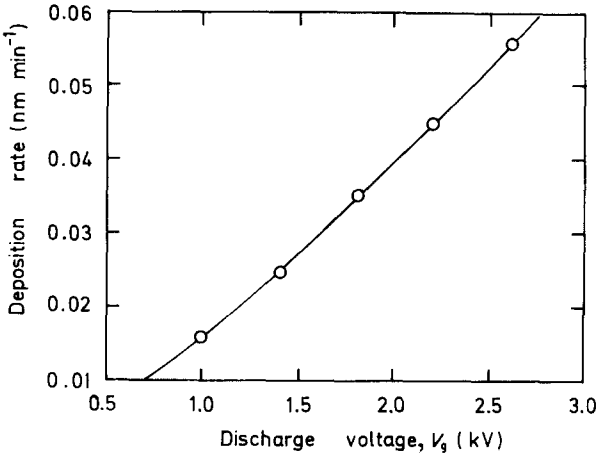

Figure 5 Measured deposition rate of a-C film versus ion-gun (discharge) voltage V_g for an ion-gun current $I_g = 220$ mA.

structural changes occurring in the metal films due to electron beam irradiation.

3. Results

3.1. Dependence of deposition rate on ion gun parameters

Measurements of the metal film deposition rate R versus I_g at constant V_g showed that $R \propto I_g$. This is illustrated in Fig. 3 which shows R versus I_g for Ni and Pt films sputtered at $V_g = 2.2$ kV. When the ion gun current I_g is changed at constant ion gun voltage V_g then the number of Ar ions bombarding the target changes but the energy of the ions is unaltered (i.e. the sputtering yield is unaltered). In this case the change in the number of ejected target atoms, and hence R, merely results from the change of bombarding ion numbers.

Fig. 4 shows the measured change in R with V_g for $I_g = 260$ mA (Ni, Pt) and $I_g = 220$ mA (Cu, Au, Ni). The corresponding graph for carbon is given in Fig. 5. The variation of R with V_g is non-linear and for particular V_g, I_g values the deposition rate increases in the sequence C < Pt < Ni < Au < Cu. This sequence is consistent with published values [14] of the normal-incidence Ar^+ sputtering yields. Changing V_g at constant I_g produces a change in the sputtering yield Y, i.e. the number of target atoms sputtered per incident Ar^+, with a consequent change in R. It is notable that the change in R with V_g (Figs 4 and 5) is not as pronounced as the change in Y with incident Ar^+ energy [14].

3.2. Metal film nucleation and growth

3.2.1. Influence of ion gun parameters

The metal film deposition rate R appropriate to a given set of ion gun parameters V_g, I_g is obtained from the experimental graphs such as those of Figs 3, 4 and 5. It is therefore possible, by adjusting the deposition time T, to obtain a set of films of identical equivalent thickness (defined as $R \times T$) deposited under a range of V_g, I_g. This was done for each of the metals Pt, Ni, Au and Cu, the equivalent thickness t' of each thin-film set being chosen to show the early discontinuous stage of film growth. For each of the metals studied the influence of V_g, I_g on the film topography was the same, so for this reason only the Pt and Au film observations will be reported.

There was no discernible difference between the TEM pictures or between the diffraction patterns of Pt films ($t' = 2.5$ nm) deposited at V_g, I_g of 2.2 kV, 220 mA and 2.2 kV, 110 mA for which $R = 0.18$ and 0.09 nm min^{-1}, respectively. Films of the same equivalent thickness t' deposited at the same I_g but different V_g did have a different appearance, however. This is illustrated in Fig. 6a and b, which show TEM pictures of Au films ($t' = 2.5$ nm) deposited at 1.2 kV, 220 mA and 2.0 kV, 220 mA, with deposition rates 0.2 and 0.37 nm min^{-1}, respectively (Fig. 4). Comparing Fig. 6a and b it is evident that the Au film deposited at the higher V_g contains fewer and larger particles than the film deposited at the lower V_g.

A quantitative comparison of these two pictures is given by the histograms of Fig. 7. These were obtained by measuring the area of each particle contained within an area 45 mm × 45 mm on the photographs (magnification 3×10^5) of Fig. 6a and b; each area contained approximately 140 particles. The histograms of Fig. 7 show that the particle area distribution in the higher V_g film peaks at ~ 40 nm^2 and is broader than that in the lower V_g film, which peaks at ~ 20 nm^2. The fractional substrate area covered by each film was found by summing the particle areas within the square; this gave coverages of $40 \pm 5\%$ and $45 \pm 5\%$ for the films deposited at 2.0 and 1.2 kV, respectively.

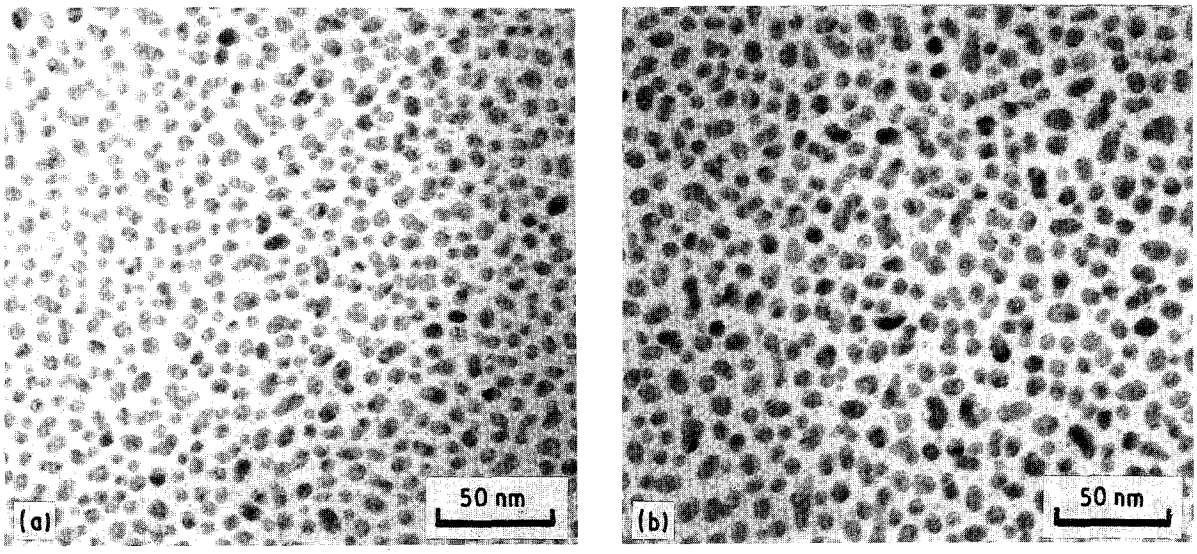

Figure 6 TEM pictures of IBS Au films ($t' = 2.5$ nm) on a-C. Sputtering parameters (a) $V_g = 1.2$ kV, $I_g = 220$ mA; (b) $V_g = 2.0$ kV, $I_g = 220$ mA.

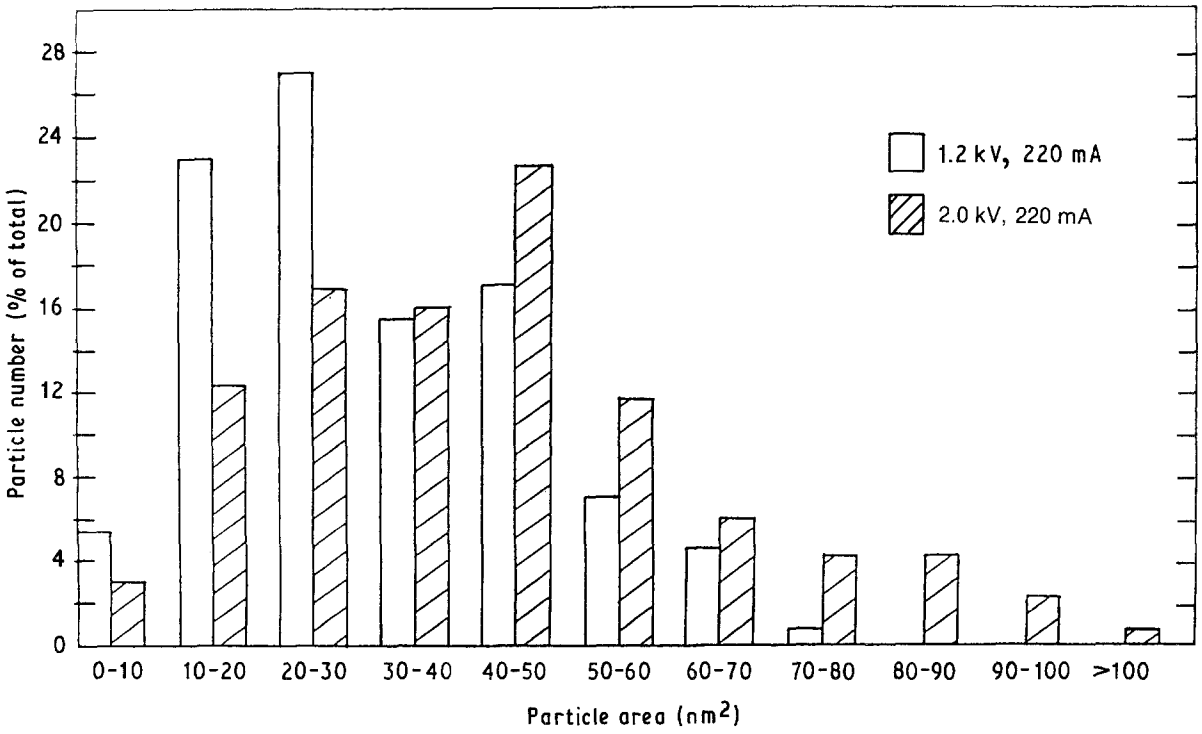

Figure 7 Particle area distribution in Au films (equivalent thickness $t' = 2.5$ nm) deposited on a-C under IBS conditions 1.2 kV, 220 mA and 2.0 kV, 220 mA.

The increase in particle area with V_g illustrated in Fig. 7 does not occur for all values of t'. At the very beginning of film growth, when the metallic islands (particles) are small and comparatively far apart, then the particle size (area) of films of the same t' deposited at different V_g are nearly the same. This situation occurs in Au films of $t' = 1$ nm, for example; the TEM picture of such an Au film is shown in Fig. 8 below.

3.2.2. Development of substrate coverage

TEM and electron diffraction pictures were taken of Au, Cu, Pt and Ni films deposited on carbon-coated EM grids using the sputtering parameters listed in Table I. For each metal a number of films, each of different equivalent thickness t', were prepared.

TEM pictures of as-deposited IBS Au films on a-C are shown in Fig. 8. When $t' = 0.5$, 1.0 and 1.5 nm the Au film consists of isolated metallic particles whose size increases with t'. In films of $t' = 2.0$ and 3.0 nm the Au particles have clustered to form short chains of irregular length and shape. When t' increases to 5.0 and 7.0 nm it is possible to see connecting paths across a large area of the film. In the Au films of $t' = 9.0$ nm the substrate is almost covered, and is completely covered when the film $t' \simeq 10$ nm, the Au grain size then being approximately 10 nm.

TABLE I Ion gun parameters (and consequent deposition rate) used in depositing the metal films, on a-C, whose TEM pictures are given in Figs 8 and 11

Metal	V_g (kV)	I_g (mA)	Deposition rate (nm min^{-1})
Pt	2.2	260	0.212
Ni	2.2	220	0.245
Cu	2.2	220	0.490
Au	2.2	220	0.420

For each of the Au film pictures shown in Fig. 8 the fraction f of the substrate surface covered by Au was estimated by measuring the perceived area of each Au particle contained within a square 45 mm × 45 mm drawn on the photographic print. These measurements are shown plotted as f versus equivalent film thickness t' in Fig. 9.

Electron diffraction patterns of the Au films of Fig. 8 consisted of a few diffuse rings in the case of the smallest t', the rings becoming sharper and more numerous as t' increased with the rings breaking up into spots at the largest t' due to the increased grain size. The d_{hkl} spacing of the crystallographic planes (hkl) giving rise to a diffraction ring of measured radius r was determined from the relation $d_{hkl} = \lambda L/r$ where λL is the known diffraction camera constant. These d_{hkl} values are listed in Table II for a thick Au film ($t' = 7$ nm) where they are compared with the calculated values based on the Au unit cell parameters [15]. The d values with an asterisk are those which were also observed in the thinnest films examined.

TEM pictures of IBS Cu films deposited on a-C substrates at room temperature are shown in Fig. 8. When the equivalent thickness t' of the Cu films is 1.0, 1.5 and 2.0 nm the film consists of isolated metal particles. With increasing t' the particles began to form chains of irregular length and shape, and when $t' = 10$ nm the substrate coverage has increased to the stage where it is possible to see connecting paths across an appreciable area of film. When $t' = 18$ nm the film contains large, regularly shaped grains and substrate coverage is complete in films of $t' = 21$ nm when the lateral grain size is approximately 15 nm. Using the procedure described earlier the fractional

TABLE II Interplanar spacings d_{meas} as determined from the electron diffraction ring pattern of a continuous metal film; values with an asterix were also evident in the thinnest film examined. Also listed are the values d_{calc} expected from the published f.c.c. unit cell parameters [15] which were used to identify the diffraction rings

(hkl)	Au (7 nm)		Cu (21 nm)		Pt (3.5 nm)		Ni (4 nm)	
	d_{calc} (nm)	d_{meas} (nm)	d_{calc} (nm)	d_{meas} (nm)	d_{calc} (nm)	d_{meas} (nm)	d_{calc} (nm)	d_{meas} (nm)
(1 1 1)	0.2355	0.0237*	0.2087	0.211*	0.2265	0.228*	0.2035	0.209*
(0 0 2)	0.2039	0.0205*	0.1808	0.182	0.1962	0.200*	0.1762	
(0 2 2)	0.1442	0.0145	0.1278	0.130	0.1387	0.140*	0.1246	0.120*
(1 1 3)	0.1230	0.0124*	0.1090	0.111*	0.1183	0.119*	0.1063	0.112*
(2 2 2)	0.1177	0.0118*	0.1044	0.107*	0.1133	0.114*	0.1017	0.104*
(0 0 4)	0.1020	0.0102	0.0904	0.0912	0.0981		0.0881	
(1 3 3)	0.0936	0.0940	0.0829	0.0836	0.0900	0.0902	0.0808	
(0 2 4)	0.0912	0.0912	0.0808	0.0814	0.0877	0.0882	0.0788	
(2 2 4)	0.0832	0.0839	0.0738	0.0742	0.0801	0.0806	0.0719	
(3 3 3), (1 1 5)	0.0785	0.0790	0.0696	0.0698	0.0755	0.0760	0.0678	
(0 4 4)	0.0721		0.0639		0.0694	0.0686	0.0630	
(1 3 5)	0.0689	0.0693	0.0610	0.0614	0.0663	0.0669	0.0596	
(0 0 6), (2 4 4)	0.0680	0.0686	0.0603	0.0608	0.0654		0.0587	
(0 2 6)	0.0645		0.0572		0.0620	0.0628	0.0557	
(3 3 5)	0.0622		0.0551		0.0598		0.0537	
(2 2 6)	0.0615	0.0617	0.0545		0.0591		0.0531	
(4 4 4)	0.0589		0.0522		0.0566		0.0509	

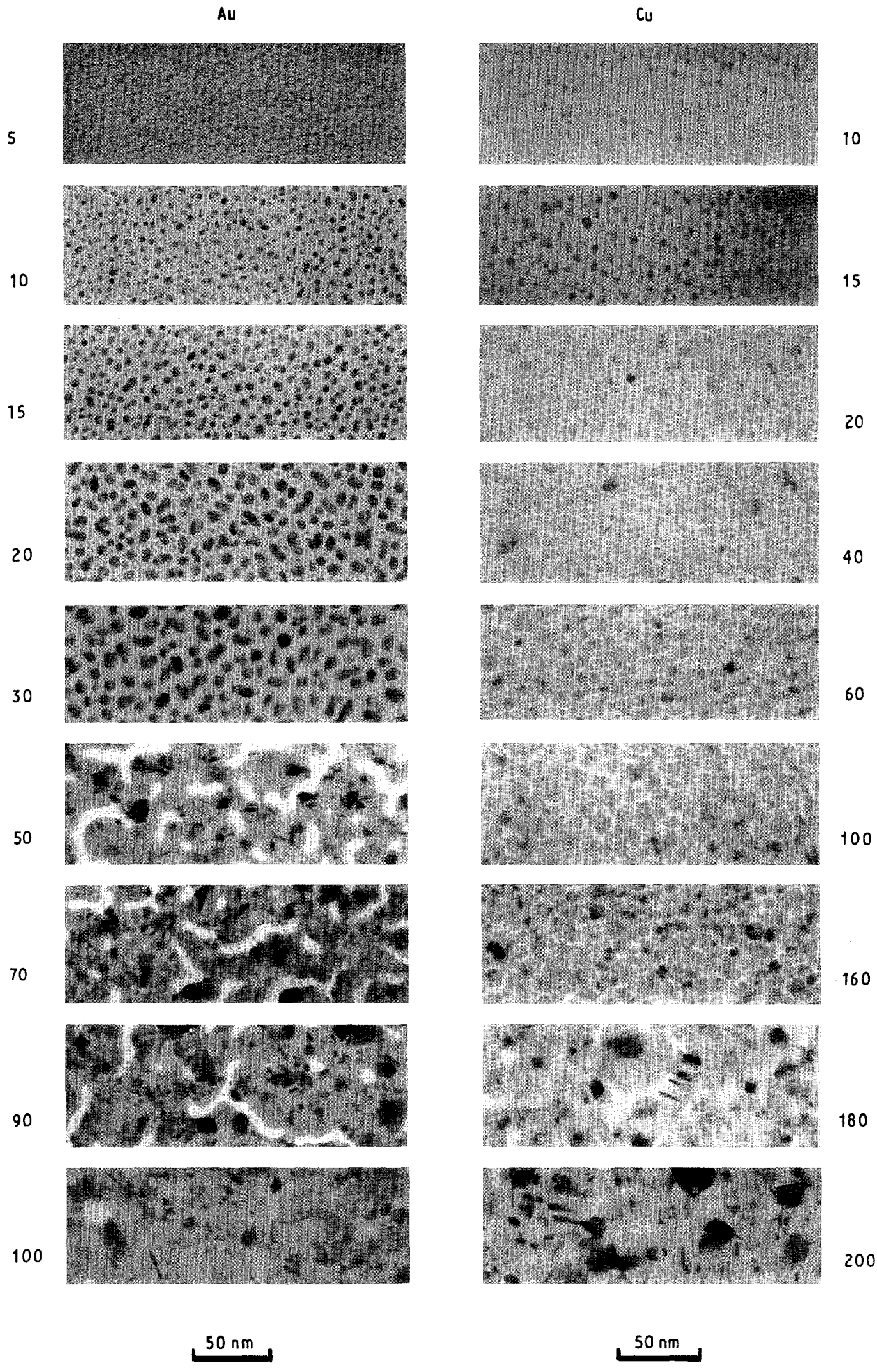

Figure 8 TEM pictures of IBS Au and Cu films on a-C. The equivalent thickness t' (nm) of each film is given in the left- and right-hand margin. The magnification scale bar is given at the foot of each picture column.

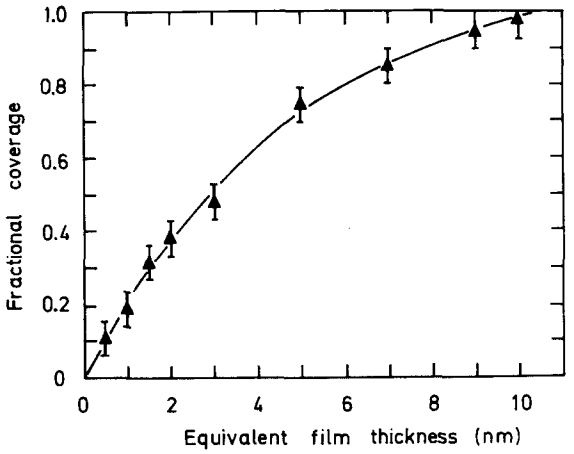

Figure 9 Fractional area coverage versus equivalent thickness of an IBS Au film (V_g = 2.2 kV, I_g = 220 mA) deposited on a-C.

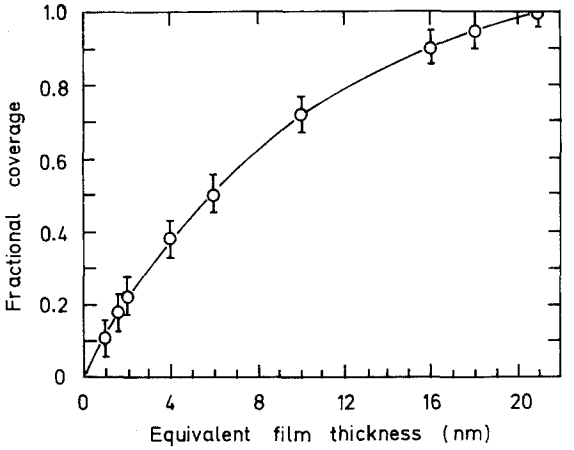

Figure 10 Fractional area coverage versus equivalent thickness of an IBS Cu film (V_g = 2.2 kV, I_g = 220 mA) deposited on a-C.

area coverage f was measured in films of different t'. These measurements are shown plotted in Fig. 10.

The d_{hkl} values of the diffraction rings observed from a thick (t' = 21 nm) Cu film are listed in Table II together with calculated values based on the f.c.c. Cu unit cell parameters [15].

TEM pictures of IBS Pt films on a-C are shown in Fig. 11. When t' = 0.5 nm the Pt film consists of isolated particles which grow to form chains of irregular length and shape when t' increases to 1.0 nm. When t' = 1.5 nm the substrate coverage has further increased and it is possible to see connecting paths across as appreciable area of film. When t' = 2.0 nm connecting paths cross the entire field of view, and the substrate coverage is almost complete when t' = 3.5 nm; at this stage the lateral dimensions of the Pt particles (grains) is approximately 4 nm. The measured increase in fractional substrate coverage f with t' is shown plotted in Fig. 12.

The interplanar d_{hkl} spacings in the thickest (t' = 3.5 nm) Pt film, as obtained from the associated electron diffraction ring pattern, are listed in Table II where they are compared with calculated values based on the Pt unit cell parameters [13].

TEM pictures of IBS Ni films on a-C are shown in Fig. 11. Compared with the Pt films of comparable t' it is evident that the Ni particles are very small and, in the case of t' = 0.5 and 1.0 nm, difficult to observe. It is just possible to recognize connecting links in Ni films of t' = 2.0 and 3.0 nm, and the substrate appears to be fully covered when t' = 4.0 nm, at which stage the particle (grain) size is $\sim$ 2 nm.

It was not possible to measure the variation of fractional substrate coverage f with t' from the Ni TEM pictures of Fig. 11, but an estimate has been obtained from the soft X-ray (λ = 0.834 nm) reflection spectra of Ni/a-C multilayers. The spectrum of one such 51/50 Ni/a-C multilayer (t'_{Ni} = 1.82 nm, $t'_{a\text{-}C}$ = 1.25 nm) is given in Fig. 13. This shows the first-order (p = 1) reflection maximum at glancing angle of incidence ϕ from which, using Equation 2, the multilayer periodicity $d = t_{Ni} + t_{a\text{-}C}$ can be determined. Since $t_{a\text{-}C}$ is known from the previously measured deposition rate (Fig. 5), so t_{Ni} is determined. A series of 51/50 Ni/a-C multilayers ($t_{a\text{-}C}$ = 1.25 nm) were prepared for which the Ni layer deposition times T were different; the multilayer spectra gave the corresponding values of t_{Ni} which allowed a graph of t_{Ni} versus T to be obtained as shown in Fig. 14. For $t_{Ni} \gtrsim 2$ nm the calibration graph coincides with the extrapolated straight-line graph obtained from measurements on the single Ni film (cf. Fig. 2), but at smaller t_{Ni} the measured values are greater than those predicted by the deposition rate. This is because the metal is now distributed as "islands" which are necessarily thicker than that of the corresponding continuous film. If it is assumed that the Ni deposition rate is constant from the very earliest stage of film growth, then the ratio of the expected (equivalent) thickness to the measured value of t_{Ni} gives a measure of the fractional substrate coverage f, shown plotted as f versus t' in Fig. 15. Note that Fig. 15 is not directly comparable with Fig 9, 10 and 11 which were obtained by direct observation.

The electron diffraction patterns of the single Ni films on a-C (Fig. 11) showed only a few diffraction rings; the derived d_{hkl} values are listed in Table II.

4. Discussion

In IBS the ion gun current I_g and voltage V_g respectively determine the number and energy of the inert gas ions bombarding the target. At the low sputtering rates employed in this investigation it was found that the metal deposition rate R was linearly proportional to I_g (Fig. 3), and varying I_g (V_g constant) had no discernible effect on the deposited particulate film morphology. The deposition rate R may also be varied by changing V_g (Fig. 4) and hence the sputtering yield Y. In this case there is an effect on the film morphology (Fig. 6).

Comparing Au films of identical equivalent thickness (2.5 nm), for example it was found that increasing V_g from 1.2 to 2.0 kV moved the peak of the particle area distribution from approximately 20 to 40 nm^2 (Fig. 7). This behaviour is similar to that observed on increasing the substrate temperature; both effects are evidently associated with the increased mobility of the metal atoms on the substrate. The influence of V_g is not apparent at the early stage of film growth, however, where the fractional substrate coverage is small.

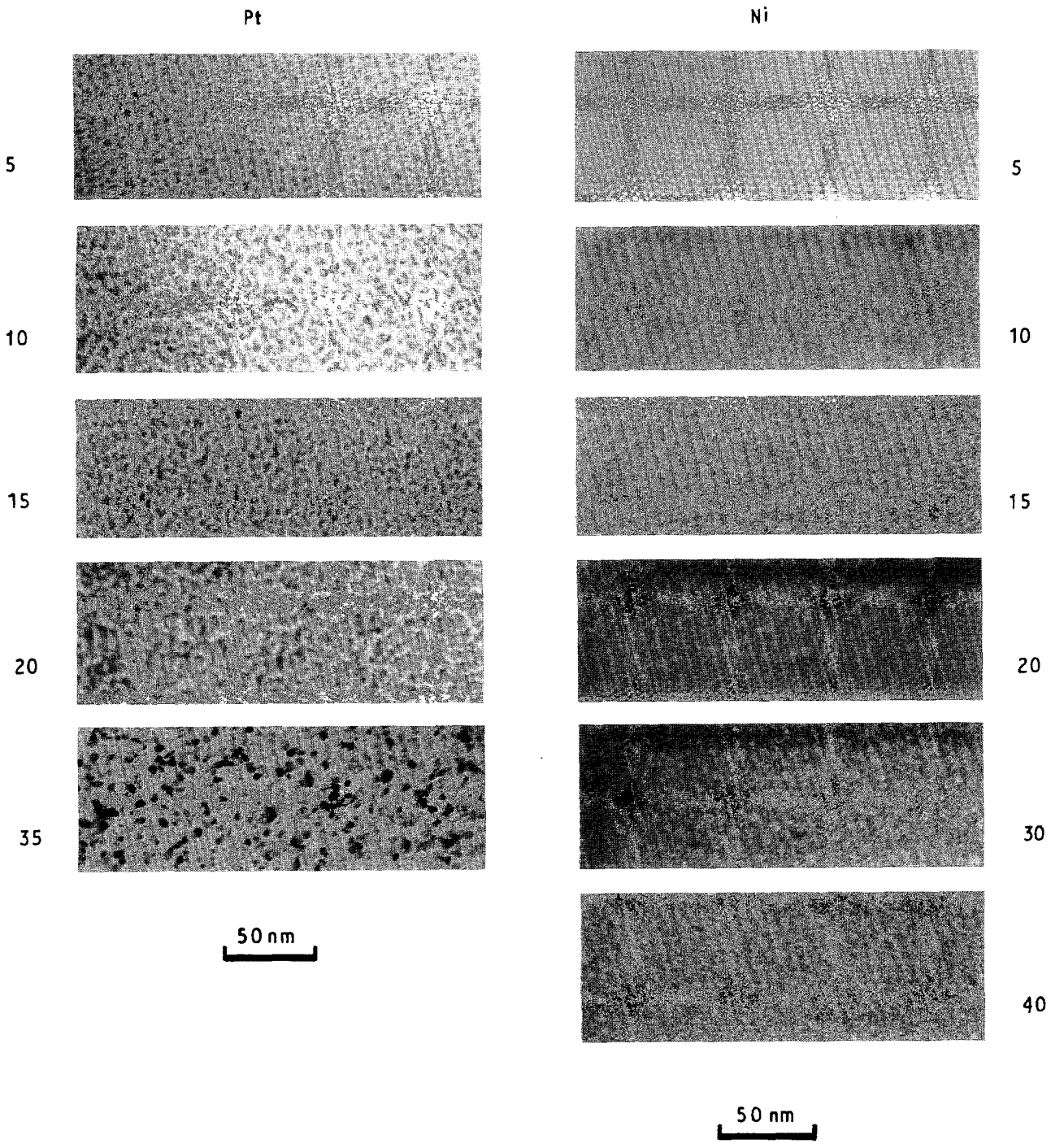

Figure 11 TEM pictures of Pt and Ni films on a-C. The equivalent thickness t' (nm) of each film is given in the left- and right-hand margin. The magnification scale bar is given at the foot of each picture column.

The TEM observations show (Figs 8 and 11) that the Au, Cu, Pt, Ni atoms arriving at the substrate initially form isolated metallic islands (nuclei). With continued deposition the islands grow in size, forming a connecting network where they come into contact and eventually completely covering the substrate. During these later stages the metallic islands have a distinct, often hexagonal, shape indicating that they are crystalline. It has been shown [16] that the equilibrium morphology of such f.c.c. microcrystals on a chemically inert substrate is consistent with the "broken bond" model which predicts the free surface energy $\gamma_{(1\,1\,1)} < \gamma_{(1\,0\,0)} < \gamma_{(1\,1\,0)}$. The electron diffraction measurements show that in the thinnest films the orientation of the f.c.c. crystals is such that (1 1 0) is parallel to the substrate; for this reason the associated $d_{h\,k\,l}$ reflections are absent (Table II). This is not the orientation expected if the metallic nuclei form by the hexagonal close packing (h.c.p.) of atoms on the substrate, four such h.c.p. layers (stacking sequence ABC/ABC) being required to form the f.c.c. unit cell (unit cell dimension a_0). In the particular case of Ni the graph of film thickness versus deposition time T (Fig. 14) appears to extrapolate to ~ 0.8 nm, which suggests that this is the minimum stable thickness of a metallic nucleus deposited at room temperature. The extrapolation is not sufficiently accurate to determine whether this minimum thickness is a multiple of h ($= a_0/3^{1/2}$) or of $6^{1/2}h/2$, i.e. the thicknesses corresponding to (1 1 1) or (1 1 0) parallel to the substrate.

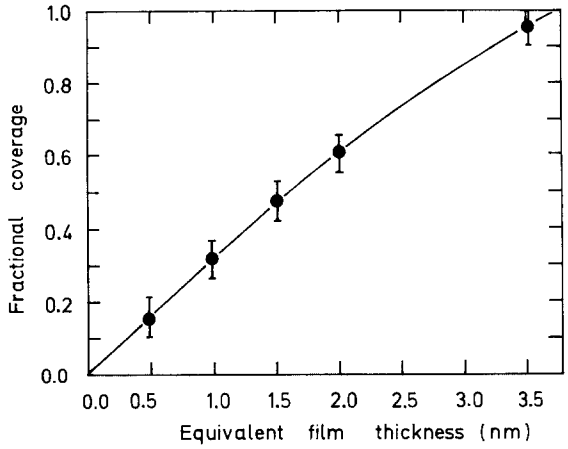

Figure 12 Fractional area coverage versus equivalent thickness of an IBS Pt film ($V_g = 2.2$ kV, $I_g = 260$ mA) deposited on a-C.

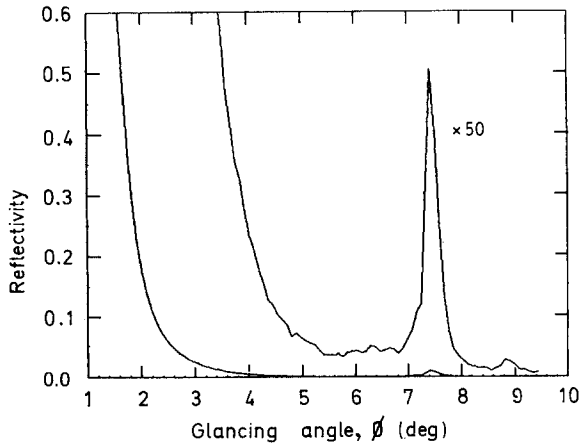

Figure 13 Measured reflectivity versus glancing angle of incidence ϕ, at wavelength $\lambda = 0.834$ nm, of a 51/50 Ni/a-C multilayer ($t'_{Ni} = 1.82$ nm, $t'_{a\text{-}C} = 1.25$ nm).

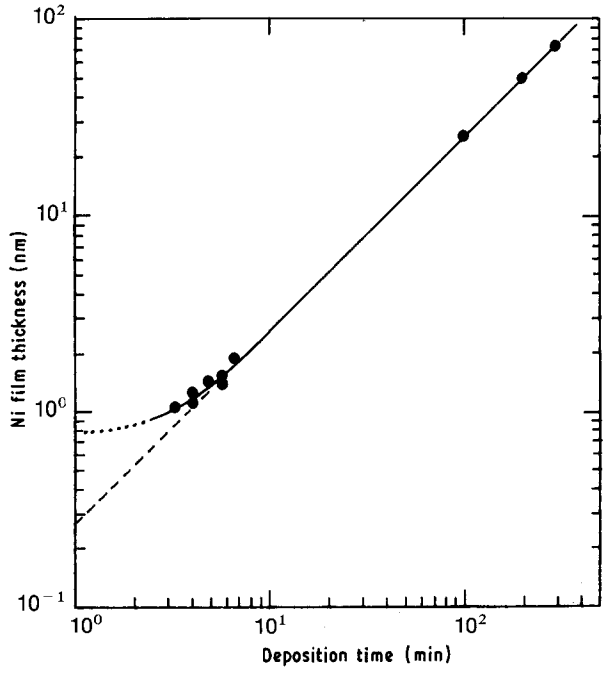

Figure 14 Measured thickness of the Ni layers in an Ni/a-C multilayer as a function of the Ni layer deposition time.

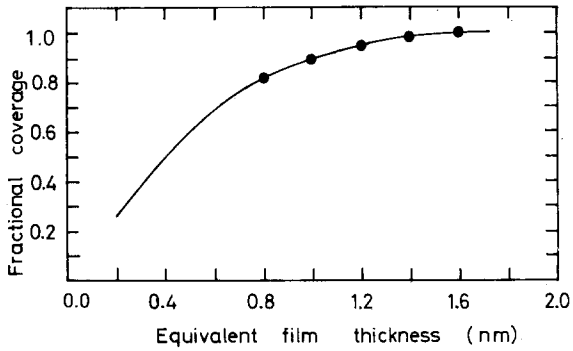

Figure 15 Area of substrate covered by an IBS Ni film compared with that covered by the same mass of material in the form of a continuous film of specified equivalent thickness.

Comparing the TEM pictures shown in Figs 8 and 11 it is seen that at the early stage of film growth, where $t' = 1.0$ nm for example, the "island" size increases in the sequence Ni, Pt, Au, Cu. If t'_1 is the equivalent thickness at which the fractional substrate coverage $f = 1$ then the TEM pictures and the graphs of Figs 15, 11, 9 and 10 show that t'_1 also increases in this sequence.

At the early stage (f small) of non-epitaxial metal film deposition it is possible to distinguish two growth modes: (i) a steady-state regime (valid if the condensation coefficient C is small) where the growth process is dominated by the diffusion of single atoms on, and evaporation from, the substrate [17, 18]; and (ii) an aggregation regime (valid when C approaches unity) where evaporation is negligible so that essentially all the deposited atoms diffuse and combine with existing islands. At the larger values of f where the islands are coalescing the atoms are deposited on to islands rather than substrate, and the situation is more of a droplet growth phenomenon [19, 20].

The IBS film deposition process is such that the early film growth stage is most likely to be that of the aggregation regime for which the rate equations have been solved using scaling theory [21]. This predicts that

(i) if no island dissociation occurs then for the three-dimensional (hemispherical) islands the time (τ) evolution of the number N of atom clusters (islands) $\propto \tau^{1/7}$, the mean cluster size $\langle S \rangle \propto \tau^{6/7}$ and the fractional coverage $f \propto \tau^{5/7}$. For flat two-dimensional islands (discs) $N \propto \ln \tau$, $\langle S \rangle \propto \tau$ and $f \propto \tau$; and

(ii) if cluster (island) dissociation can occur up to a critical cluster size of m atoms, then N approaches a finite value and growth proceeds by increasing island size; $\langle S \rangle \propto \tau$, rather than N. In this case, for flat islands $f \propto \tau$ while for three-dimensional islands $f \propto \tau^{2/3}$.

The possible growth modes within the aggregation regime are all described by the general relation $f \propto \tau^{\alpha}$ where $\alpha = 1$ for two-dimensional islands or $\alpha = 2/3$ or 5/7 for three-dimensional islands, depending upon whether island dissociation does or does not occur. Plotting the experimental values of f versus equivalent thickness t' for Au, Cu and Pt films (shown in Figs 9,

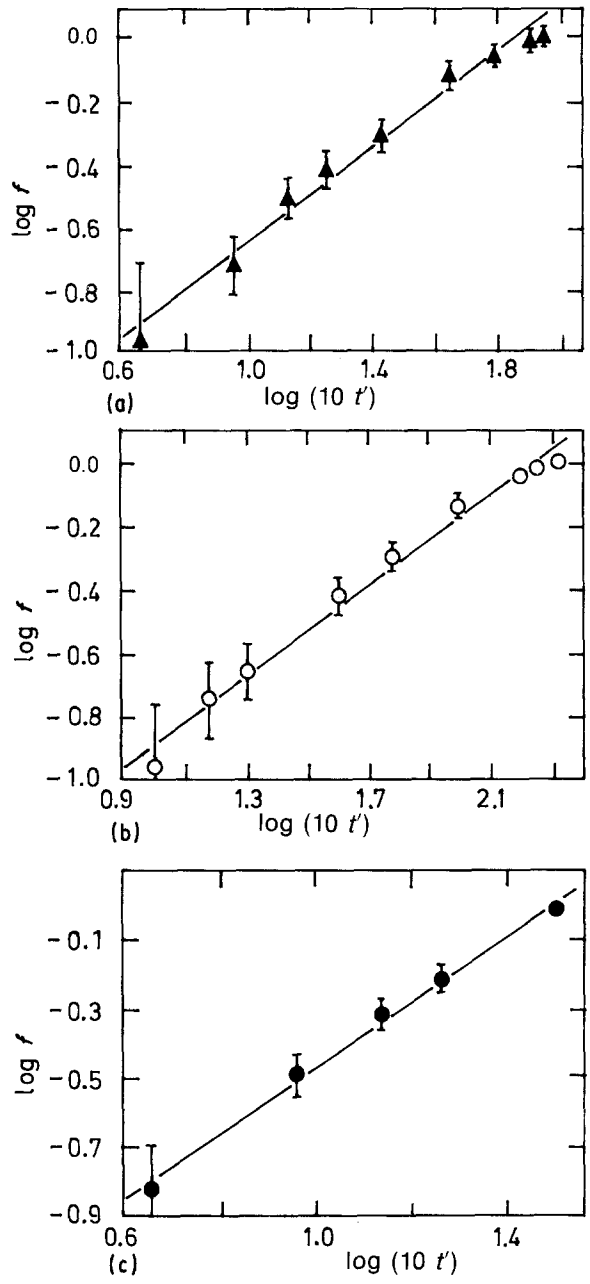

Figure 16 Measured fractional coverage f of (a) Au, (b) Cu and (c) Pt films of equivalent thickness t' deposited on a-C (Figs 9, 10 and 12), plotted as log f versus log ($10t'$).

10 and 12) in the form of log f versus log t' (Fig. 16), it is seen that the relation $f \propto \tau^{\alpha}$ applies over the major part of the range $f < 1$ with $\alpha = 0.7 \pm 0.1$ for Au and Cu and $\alpha = 0.9 \pm 0.1$ for Pt films. This suggests that the Au and Cu islands adopt three-dimensional growth whereas the Pt islands are two-dimensional (disc-like). The graph of f versus t' for Ni (Fig. 15) does not extend over a large enough range of f to enable the value of α to be determined.

It is not possible to determine the nucleation rate from the TEM pictures of Figs 8 and 11, since even in the most favourable case, that of Au on a-C, it is evident that agglomeration is occurring at an early stage, $t' = 1.5$ nm. In addition it has been shown, in the case of Au on KCl, that sub-microscopic atom clusters may be present whose presence can be revealed by subsequent Cd atom deposition [22].

It is evident from the TEM pictures of Figs 8 and 11 that the nucleation and growth of Au and Cu films are similar to each other but different from that of Pt and Ni, which cover the substrate at much smaller equivalent thicknesses than Au and Cu. This supports the conclusion drawn from the graphs of Fig. 16, namely that Pt (and presumably Ni) grow as flat two-dimensional clusters rather than three-dimensional ones. In this context it is interesting that the soft X-ray spectra of Ni/a-C and Pt/a-C multilayers [23] indicate that the metal islands have well-defined thicknesses which are an integer number of atomic diameters (Fig. 14).

References

1. J. A. VENABLES, G. D. T. SPILLER and M. HANBÜCKEN, *Rep. Prog. Phys.* **47** (1984) 399.
2. K. REICHELT, *Vacuum* **38** (1988) 1083.
3. M. VOLMER, "Kinetik der Phasenbildung" (Steinkopf, Dresden, 1939).
4. F. C. FRANK and J. H. van de MERWE, *Proc. R. Soc. A* **198** (1949) 205.
5. *Idem, ibid.* **200** (1949) 125.
6. *Idem, ibid.* **201** (1950) 261.
7. I. N. STRANSKI and L. KRASTANOV, *Sitzber. Akad. Wiss. Wien, Math-Naturw. K*1 *Abt. II B* **146** (1938) 797.
8. I. MARKOV and R. KAISCHEW, *Krist. Techn.* **11** (1976) 685.
9. D. KASHCHIEV, J. P. van der EERDEN and C. van LEEUWEN, *J. Cryst. Growth* **40** (1977) 47.
10. B. GRUZZA and E. GILLET, *Thin Solid Films* **68** (1980) 345.
11. J. DERRIEN, F. ARNAUD D'AVITAYA and M. BIENFAIT, *Rev. Phys. Appl.* **11** (1976) 377.
12. H. BETHGE, *Phys. Status Solidi* **2** (1962) 3.
13. B. L. HENKE, *AIP Conf. Proces.* No. 75 (1981) 146.
14. H. H. ANDERSON, H. L. BAY, R. BEHRISH, M. T. ROBINSON, H. E. ROOSENDAAL and P. SIGMUND, in "Sputtering by Particle Bombardment", edited by R. Behrisch (Springer Verlag, New York, 1981) p. 176.
15. J. W. EDINGTON, "Practical Electron Microscopy in Materials Science", Vol. 2 (Macmillan, London, 1975).
16. B. E. SUNDQUIST, *Acta Metall.* **12** (1964) 67.
17. M. HARSDORFF, *Thin Solid Films* **90** (1982) 1.
18. J. A. VENABLES, *Phil. Mag.* **27** (1973) 697.
19. K. BINDER and D. STAUFFER, *Adv. Phys.* **25** (1976) 343.
20. P. G. J. van DONGEN and M. H. ERNST, *Phys. Rev. Lett.* **54** (1985) 1396.
21. J. A. BLACKMAN and A. WILDING, *Europhys. Lett.* **16** (1991) 115.
22. H. BETHGE, *Phys. Status Solidi* **2** (1962) 3.
23. B. L. EVANS and B. J. KENT, *Appl. Optics* **26** (1987) 4491.

Received 18 April
and accepted 7 June 1991